Title

Investigation of SiOx anode fading mechanism with limited capacity cycling

Journal

APL Materials, 10(1)

ISSN

2166-532X

Authors

Xiao, Haiqing

Fang, Chen

Zheng, Tianyue

et al.

Publication Date

2022

DOI

10.1063/5.0077036

Peer reviewed

APL Materials

Investigation of SiO_x anode fading mechanism with limited capacity cycling

Cite as: APL Mater. **10**, 011108 (2022); https://doi.org/10.1063/5.0077036
Submitted: 29 October 2021 • Accepted: 26 December 2021 • Published Online: 13 January 2022

Haiqing Xiao, Chen Fang, Tianyue Zheng, et al.

Investigation of SiO_x anode fading mechanism with limited capacity cycling

Cite as: APL Mater. 10, 011108 (2022); doi: 10.1063/5.0077036
Submitted: 29 October 2021 • Accepted: 26 December 2021 •
Published Online: 13 January 2022

Haiqing Xiao,[1,2] Chen Fang,[1] Tianyue Zheng,[1] Hua Bai,[2,a)] and Gao Liu[1,a)]

AFFILIATIONS

[1] Energy Storage and Distributed Resources Division, Lawrence Berkeley National Laboratory, 1 Cyclotron Road, Berkeley, California 94720, USA

[2] Institute of Industrial and Consumer Products Safety, Chinese Academy of Inspection and Quarantine (CAIQ), No. 11 Ronghua South Road, Beijing 100176, China

Note: This paper is part of the Special Topic on Abundant and Non-Toxic Materials for Batteries.
[a)]**Authors to whom correspondence should be addressed:** baih111@sina.com and gliu@lbl.gov

ABSTRACT

Silicon suboxide (SiO_x) is one of the promising anode materials for the next-generation lithium-ion batteries. However, SiO_x has a severe capacity fading problem during cycling. It is thus desired to investigate the detailed fading mechanisms of SiO_x anode materials. In this study, limited capacity cycling was employed to examine the electrochemical behaviors of the SiO_x anode, and the lithiation/delithiation cycling was limited within a range of 10% theoretical capacity. This strategy minimizes the volume variation of SiO_x materials upon charging/discharging, which helps to reveal their decay factors other than volume fluctuation. It is demonstrated that the instability of the SiO_x surface during cycling was likely a parallel factor of active material fading, which seems to cause unfavored electrode interface rearrangements with lowered electric conductivity.

I. INTRODUCTION

Lithium-ion batteries (LIBs) have been extensively applied in daily electronics and electric vehicles (EVs) due to their good operational stability as well as high energy densities.[1–4] The rapid increase of energy storage demands has motivated a lot of research targeting novel battery systems, such as lithium–sulfur batteries[5–8] and lithium–air batteries.[9,10] However, on the other hand, next-generation LIBs with enhanced energy densities enabled by high-capacity active materials are still promising candidates.[11,12] In particular, silicon (Si) is a competitive anode material for LIBs because it theoretically has over ten-fold capacity (~4200 mAh/g) as that of widely used graphite anode materials (~370 mAh/g).[13,14] Nevertheless, the practical deployment of Si anodes is still confronted with critical challenges, such as severe volume swelling (~300%) and unstable solid electrolyte interphase (SEI) during repetitive lithiation–delithiation cycles that could readily result in rapid capacity fading.[12,15] Researchers have developed nanostructured materials and composite materials for Si-based anodes, which delivered improved electrochemical performance.[16,17] However, the problems of large volume change, unstable SEI, and consumption of lithium still hinder the large-scale utilization of Si anodes.[3] Silicon suboxides (SiO_x, $x < 2$) are a class of alternative silicon anode materials that have attracted wide research interest. The key advantage of SiO_x anode materials is their relatively improved cycling stability in comparison to silicon anodes, which benefits from the irreversible formation of lithium oxide and lithium silicate during initial lithiation that could serve as a volume buffer matrix for the active materials in subsequent electrochemical reactions.[3,18,19] Despite these positive factors, SiO_x would still experience a volume expansion of 100%–150% upon electrochemical lithiation.[20,21] In addition, SiO_x also has a similar capacity fading issue to that of Si materials.[18] The possible causes include particle pulverization, repetitive SEI growth, volume change during full-depth charge/discharge, and loss of electric contact between active materials and the current collector.[22–26]

Si-based anodes face a common problem of unstable interface during charge–discharge cycling.[3] Considerable research effort

has been made to enhance silicon electrode surface properties. For example, fluoroethylene carbonate (FEC) additive has been widely employed to improve the performance of Si-based electrodes.[27–31] The FEC additive generally promotes the generation of a uniform and stable SEI layer to suppress continuous electrolyte decomposition at the electrode surface. However, on the other hand, there have also been reports showing higher cell performance with non-FEC electrolytes.[3,32] To demonstrate the differences in electrode surface properties, long-term cycling is often performed,[33–35] which is time-consuming. To make it worse, the fading of Si-based electrodes could depend on a series of factors, with the dramatic volume changes very possibly playing the major role.[36–38] Thus, it is challenging to individually investigate the impact of Si surface evolution or to evaluate the effectiveness of a given electrode interface improvement strategy. Due to the chemical complexity of battery systems, it is desirable to develop specialized analytical approaches for characterization of battery electrochemistry.[39–43] In this study, the electrochemical behavior of SiO_x electrodes was investigated with limited capacity cycling (lithiation–delithiation within 10% theoretical capacity). Such a cycling protocol could reduce the 100%–150% volume expansion of SiO_x to roughly 10%–15% level, which is comparable to that of graphite[44] at about 13%. With the volume expansion factor largely eliminated, the contribution of silicon interface evolution in electrode fading was demonstrated. Electrochemical impedance spectroscopy (EIS)[45] is a powerful technique in LIB studies to investigate SEI statuses, insertion/de-insertion reactions, and diffusion behaviors. The evolution of SiO_x anodes was characterized by EIS as well as morphology measurements. The limited capacity cycling proves to be a facile testing strategy to investigate silicon electrode decay factors other than volume expansion.

II. MATERIALS AND METHODS

A. Materials

Styrene-butadiene rubber (SBR) emulsion (JSR TRD105A, 40.7 wt. %) was obtained from JSR Corporation, Japan. Carboxymethyl cellulose sodium salt (CMC, Mw 250000, D. S. 0.90) was obtained from Aldrich. TIMCAL SUPER C65 was used as a conductive carbon agent. Micrometer-sized SiO_x was obtained from Bosch. The $LiNi_{0.5}Mn_{0.3}Co_{0.2}O_2$ (NMC532) cathode was provided by Argonne National Laboratory (ANL).

B. Electrode preparation

The electrode preparation followed the strategy in a previous report[46] and is briefly summarized as follows. Pre-mixing of SiO_x, C65, and CMC was performed with ball milling in water for 6 h. After addition of SBR, the mixture was further ball-milled overnight. Then, the slurry was cast onto copper foil to make the electrode film (compressed to 40 μm thickness) with a final composition of SiO_x/C65/CMC/SBR (80/10/5/5, w/w).

C. Cell testing

Cells of silicon electrodes were assembled in an argon-filled glovebox with 2325 coin cells and 1.2M $LiPF_6$ ethylene carbonate:diethyl carbonate (EC:DEC, 1:2 w/w) electrolyte (Li foil or NMC532 counter electrodes). The coin cell performance was evaluated in a thermal chamber at 30 °C with a Maccor Battery Test System. Electrochemical impedance spectroscopy (EIS) was performed in EC-Lab with frequencies ranging from 20 kHz to 10 mHz, and the perturbation signal was 10 mV. Morphology characterization of electrodes was performed with a JSM-7500F (JOEL Ltd.) scanning electron microscope (SEM). Before-cycling SEM data were obtained previously.[47]

III. RESULTS AND DISCUSSION

A. Half cell performance with limited capacity cycling

First, limited capacity cycling was applied to the SiO_x electrode in half cell testing. The initial cycle was carried out with full lithiation followed by delithiation to 40% theory capacity. The subsequent cycles underwent repetitive lithiation/delithiation within the range of 10% theory capacity at the rate of 1 C (1.3 A/g), and the cycling capacities are presented in Fig. 1. The voltage changes of the half cell during cycling are shown in Fig. 2. The gap between the high voltage and low voltage could serve as an indicator for the cell status. It can be observed that the gap between the high voltage and low voltage was expanding during cycling. In particular, the high voltage initially increased slowly from the starting point to around 230 h, corresponding to nearly 450 cycles; then, the high voltage quickly climbed above 1.5 V (hitting the high voltage limit of the cycling protocol), which implies that the cell could no longer cycle properly. That is to say, the cell has decayed to a failure point after about 450 cycles of limited capacity cycling (10% capacity lithiation/delithiation).

B. Full cell performance with limited capacity cycling

In half cells, the lithium counter electrodes may also decay during cycling, which could be challenging to distinguish from the fading of the silicon electrodes. Therefore, further studies are needed to verify the role of silicon electrode degrading. To pursue this goal, a commercially available and stable cathode, NMC532, was used to fabricate full cells. The formation cycles were carried out with charge–discharge at C/25 rate (1 C = 1.3 A/g) for 4 cycles. Then, the cell was charged to 50% theory capacity, followed by 10% theory capacity discharge–charge cycling under 1 C rate. The potential limiting window was 2.8–4.0 V vs Li/Li^+. The cycling capacities

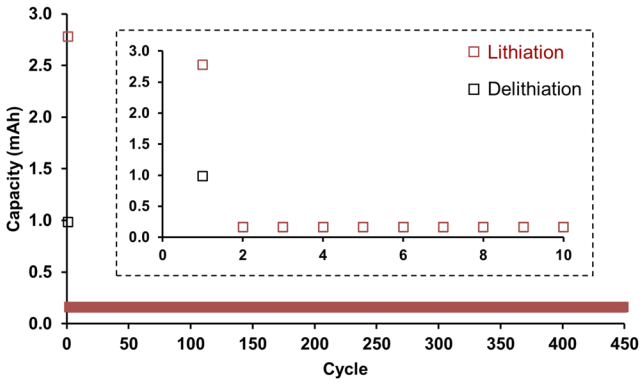

FIG. 1. The cycling capacities of the SiO_x half cell. The inset demonstrates the charge/discharge capacities during the initial cycles.

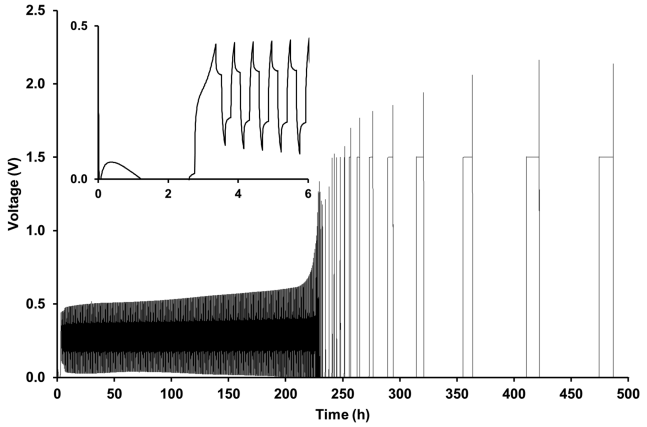

FIG. 2. The voltage changes of the SiO_x half cell during cycling. The inset demonstrates the voltage profile during the initial hours.

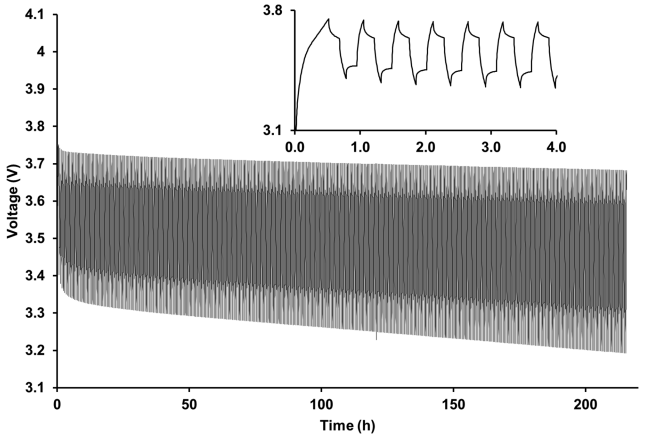

FIG. 4. The voltage changes of the SiO_x full cell during cycling. The inset demonstrates the voltage profile during the initial hours.

are presented in Fig. 3, and the voltage changes during 10% capacity cycling are shown in Fig. 4 (Fig. 4 starts with the fifth cycle, namely, after the formation cycles). Similar to the case of the half cell, the trend of high voltage and low voltage could also illustrate the properties of the electrodes during cycling. Figure 4 demonstrates an expanding gap between the high voltage and low voltage during cycling, indicating gradual fading of the cell. To be more specific, during the course of 215 h cycling, the high voltage decreased slowly from 3.75 to 3.68 V, and the low voltage decreased faster from around 3.4 to 3.2 V. These results indicated that the cathode maintained its stability during cycling while the anode clearly experienced outstanding performance fading.

C. Impedance of SiO_x full cell during cycling

The voltage profile during cycling is a convenient marker to identify cell decay, and additional characterization is demanded to reveal the fading mechanism of the cell. Generally, continuous SEI reactions associated with severe volume changes during charge–discharge cycling are considered the major causes for fading of SiO_x anodes.[3] In this study, the anodes only underwent discharge–charge cycling over a limited range of 10% theoretical capacity, during the process of which the volume change would be non-outstanding (comparable to that of graphite) and the SEI would not be significantly disturbed by SiO_x volume fluctuation. However, the expanding gaps between the high voltages and the low voltages in both half cell and full cell clearly demonstrated gradual degrading of the SiO_x electrodes during the limited capacity cycling.

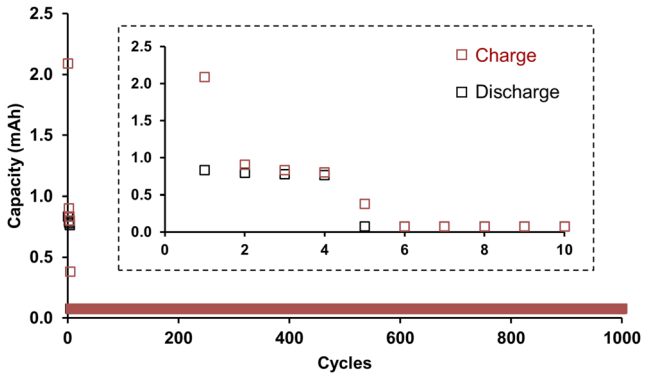

FIG. 3. The cycling capacities of the SiO_x full cell. The inset demonstrates the charge/discharge capacities during the initial cycles.

EIS was employed to further investigate the fading mechanism. For the EIS measurement, the full cell was processed identically as that for cycling (four formation cycles at C/25), and the impedance was measured every 20 cycles at 40% theory capacity (discharged state) during repeated 10% capacity cycling at 1 C rate. The measurements were sequentially labeled as Ipd1 through Ipd10. As shown in Fig. 5, for each curve, two semicircles and a straight line were clearly observed in the Nyquist plot, and the equivalent circuit diagram[48,49] is provided. The components of the circuit are explained as follows. The bulk resistance R_b is contributed by cell parts, such as electrodes, electrolyte, and current collectors; the Ohmic resistance of the surface layer, namely, R_{sl}, corresponds to the resistance of SEI; R_{ct} reflects the charge transfer resistance of electrode reactions; Warburg impedance (Z_W) is associated with the lithium diffusion in the electrode. The two semicircles located in the high-frequency and middle-frequency ranges are attributed to lithium-ion transportation in the SEI film (R_{sl}) and the charge transfer resistance at amorphous silicon domains (R_{ct}), respectively, and the straight line at the low frequency is generated by lithium diffusion in the particles, namely, Warburg impedance (Z_W). There is no significant change in the semicircle radius at the high frequency in the EIS spectra shown in Fig. 5. It can be deduced that the SEI remained stable during the cycling. There is also no significant change in the straight line at the low frequency, which indicates that the diffusion resistance in the particles remained steady during cycling. It is obvious that the radius of the semicircle at the medium frequency continuously becomes larger from Ipd1 to Ipd10, which indicates that the charge-transfer

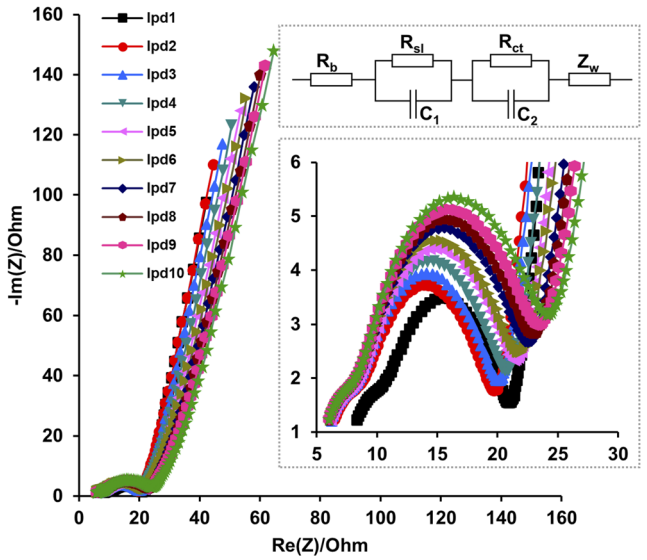

FIG. 5. Electrochemical impedance spectroscopy of the SiO_x full cell during cycling (insets show the equivalent circuit diagram and expanded spectra in the high frequency range).

resistance at amorphous Si domains became higher and higher during cycling. In other words, the electrical conductivity of the anodes became worse during cycling. Further discussions are provided in Sec. III D in combination with morphology characterization of the electrode.

D. Surface morphology of SiO_x anodes

To provide additional information regarding the SiO_x material evolution during cycling, morphology measurements were carried out. SEM analysis was employed to examine the microstructure of the SiO_x electrode before and after cycling in the full cell to further demonstrate the fading process of the anode. Figures 6(a) and 6(b) vs Figs. 6(d) and 6(e) illustrate that the anode surface does not present noticeable cracks after cycling, and the smooth anode film (before cycling) only turned slightly roughened (after cycling). In addition, the SiO_x particles have sharp edges prior to cycling [Fig. 6(c)], while the particle edges are rounder and the particle surfaces present minor fuzziness after cycling [Fig. 6(f)]. These are typical contrasts of the silicon anode before and after cycling, although the changes here are relatively minor compared to silicon anodes cycled in full capacity depth.[46] These observations demonstrate that the limited volume expansion during 10% capacity cycling did not lead to apparent damages of the electrode, which verified the effectiveness of the limited capacity cycling strategy to avoid the extensive volume changes of SiO_x materials.

In addition to the morphology changes of the particle surfaces, the conductive additive distribution was also different after cycling. There were fewer conductive agents on the active materials after cycling than before cycling [Figs. 6(c) and 6(f)]. Such an observation demonstrates that the electric conductivity of the anode decreased upon cycling, which agrees with the EIS results (Fig. 5). It is very likely that the loss of electric contact between active particles was one of the key factors causing SiO_x anode fading. Since the SiO_x particles did not undergo significant volume variation during the 10% capacity charge/discharge, the evolution of the SiO_x particle surfaces was largely associated with their intrinsic properties. The results revealed that the instability of the SiO_x surface likely led to unfavored rearrangements of the interface, which was a cause for anode fading. This fading factor of SiO_x active materials was investigated separately here from the volume variation factor and has been confirmed individually. It can explain for the higher charge transfer resistance on the anode side after cycling as observed in Fig. 5. It is worth briefly noting that a series of solutions have been proposed to address the silicon interface instability issue, such as surface decoration to reduce electrolyte contact with silicon particles,[50,51] nanostructured coating at the Si surface to increase

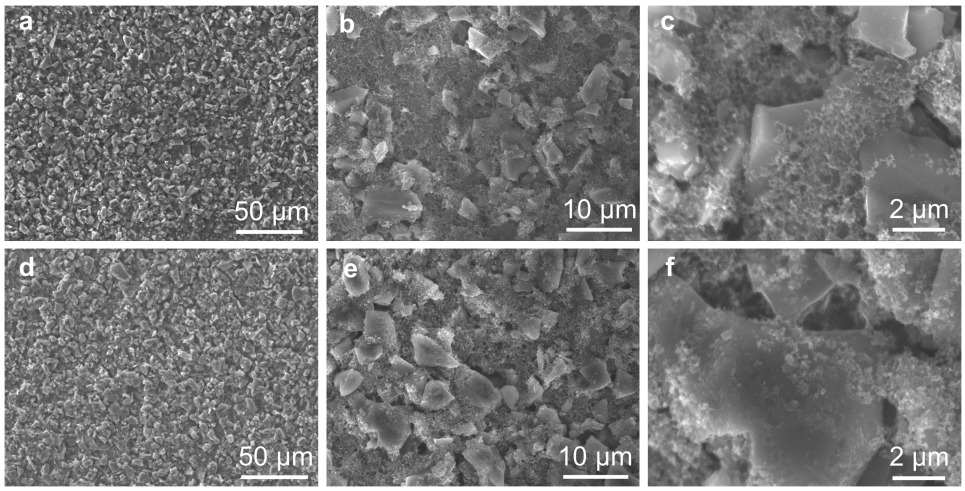

FIG. 6. SEM images of the SiO_x anode before and after cycling (full cell). (a)–(c) Images of the SiO_x anode before cycling. (d)–(f) Images of the SiO_x anode after cycling.

conductivity,[52,53] and robust artificial SEI to protect the silicon interface.[54]

IV. CONCLUSION

This work demonstrates a simple and effective approach for investigating the SiO_x anode fading mechanism under the condition of suppressed volume expansion of the active materials. It was realized by limiting the cell lithiation–delithiation cycles within the range of only 10% theoretical capacity of the active materials (limited capacity cycling). Such a strategy could minimize the volume change of silicon materials and thus allow identification of parallel fading factors of SiO_x anodes other than volume fluctuation. The behaviors of SiO_x anodes were examined in both half cell and full cell setups. The voltage profiles of the cells showed gradually expanding gaps between the high voltages and low voltages, which served as indicators of the cell condition and reflected the fading of SiO_x electrodes. The precise causes for the decay of active materials without undergoing large volume changes were further investigated by impedance and morphology measurements. The impedance spectra showed that the charge transfer resistance presented a continuously increasing trend during limited capacity cycling. The morphology comparison of the electrode before and after cycling supported the above observation, where the surfaces of the particles were found to be rougher after cycling with reduced coverage of conductive carbon agents. The limited capacity cycling strategy excluded the volume variation factor of SiO_x materials and revealed that the intrinsically unstable interfaces of the active materials could present unfavored evolution during cycling processes, which is likely one of the factors causing SiO_x anode fading.

ACKNOWLEDGMENTS

This work was supported by the Assistant Secretary for Energy Efficiency, Vehicle Technologies Office of the U.S. Department of Energy, under the Silicon Consortium Program. Electron microscopy experiments were conducted at the National Center for Electron Microscopy (NCEM) of the Molecular Foundry in Lawrence Berkeley National Laboratory. Work at the Molecular Foundry was supported by the Office of Science, Office of Basic Energy Sciences, of the U.S. Department of Energy under Contract No. DE-AC02-05CH11231. H.X. acknowledges support from the National Key R and D Program of China (Grant No. 2017YFF0210703).

AUTHOR DECLARATIONS

Conflict of Interest

The authors have no conflicts to disclose.

Author Contributions

H.X. and C.F. contributed equally to this work.

DATA AVAILABILITY

The data that support the findings of this study are available from the corresponding authors upon reasonable request.

REFERENCES

[1] R. Xiong, Y. Pan, W. Shen, H. Li, and F. Sun, Renewable Sustainable Energy Rev. **131**, 110048 (2020).
[2] C. Fang, Z. Liu, J. Lau, M. Elzouka, G. Zhang, P. Khomein *et al.*, J. Electrochem. Soc. **167**, 020506 (2020).
[3] T. Chen, J. Wu, Q. Zhang, and X. Su, J. Power Sources **363**, 126–144 (2017).
[4] C. Fang, J. Lau, D. Hubble, P. Khomein, E. A. Dailing, Y. Liu *et al.*, Joule **5**, 415–428 (2021).
[5] C. Fang, G. Zhang, J. Lau, and G. Liu, APL Mater. **7**, 080902 (2019).
[6] Z. Liu, X. He, C. Fang, L. E. Camacho-Forero, Y. Zhao, Y. Fu *et al.*, Adv. Funct. Mater. **30**, 2003605 (2020).
[7] Y. Zhao, C. Fang, G. Zhang, D. Hubble, A. Nallapaneni, C. Zhu *et al.*, Front. Chem. **8**, 484 (2020).
[8] Z. Li, C. Fang, C. Qian, S. Zhou, X. Song, M. Ling *et al.*, ACS Appl. Polym. Mater. **1**, 1965–1970 (2019).
[9] X. Lei, X. Liu, W. Ma, Z. Cao, Y. Wang, and Y. Ding, Angew. Chem., Int. Ed. **57**, 16131–16135 (2018).
[10] Z. Guo, C. Li, J. Liu, Y. Wang, and Y. Xia, Angew. Chem., Int. Ed. **56**, 7505–7509 (2017).
[11] P. Li, H. Kim, S.-T. Myung, and Y.-K. Sun, Energy Storage Mater. **35**, 550–576 (2021).
[12] S. Zhou, C. Fang, X. Song, and G. Liu, Batteries Supercaps **4**, 240–247 (2021).
[13] M. Gu, Y. He, J. Zheng, and C. Wang, Nano Energy **17**, 366–383 (2015).
[14] S. Zhou, C. Fang, X. Song, and G. Liu, Carbon Energy **2**, 143–150 (2020).
[15] J. Liu, P. Kopold, P. A. van Aken, J. Maier, and Y. Yu, Angew. Chem., Int. Ed. **54**, 9632–9636 (2015).
[16] Y. Chen, S. Zeng, J. Qian, Y. Wang, Y. Cao, H. Yang *et al.*, ACS Appl. Mater. Interfaces **6**, 3508–3512 (2014).
[17] D. S. Jung, T. H. Hwang, S. B. Park, and J. W. Choi, Nano Lett. **13**, 2092–2097 (2013).
[18] X. Feng, J. Yang, X. Yu, J. Wang, and Y. Nuli, J. Solid State Electrochem. **17**, 2461–2469 (2013).
[19] H. Takezawa, S. Ito, H. Yoshizawa, and T. Abe, Electrochim. Acta **245**, 1005–1009 (2017).
[20] T. Kang, J. Chen, Y. Cui, Z. Wang, H. Xu, Z. Ma *et al.*, ACS Appl. Mater. Interfaces **11**, 26038–26046 (2019).
[21] S. C. Jung, H.-J. Kim, J.-H. Kim, and Y.-K. Han, J. Phys. Chem. C **120**, 886–892 (2016).
[22] M. Jiao, Y. Wang, C. Ye, C. Wang, W. Zhang, and C. Liang, J. Alloys Compd. **842**, 155774 (2020).
[23] Z. Liu, Q. Yu, Y. Zhao, R. He, M. Xu, S. Feng *et al.*, Chem. Soc. Rev. **48**, 285–309 (2019).
[24] P. Li, G. Zhao, X. Zheng, X. Xu, C. Yao, W. Sun *et al.*, Energy Storage Mater. **15**, 422–446 (2018).
[25] Q. Yuan, F. Zhao, Y. Zhao, Z. Liang, and D. Yan, J. Solid State Electrochem. **18**, 2167–2174 (2014).
[26] U. Kasavajjula, C. Wang, and A. J. Appleby, J. Power Sources **163**, 1003–1039 (2007).
[27] N.-S. Choi, K. H. Yew, K. Y. Lee, M. Sung, H. Kim, and S.-S. Kim, J. Power Sources **161**, 1254–1259 (2006).
[28] H. Jia, L. Zou, P. Gao, X. Cao, W. Zhao, Y. He *et al.*, Adv. Energy Mater. **9**, 1900784 (2019).
[29] V. Etacheri, O. Haik, Y. Goffer, G. A. Roberts, I. C. Stefan, R. Fasching *et al.*, Langmuir **28**, 965–976 (2012).
[30] F. An, H. Zhao, W. Zhou, Y. Ma, and P. Li, Sci. Rep. **9**, 14108 (2019).
[31] E. Markevich, G. Salitra, and D. Aurbach, ACS Energy Lett. **2**, 1337–1345 (2017).
[32] X. Zhao and V.-P. Lehto, Nanotechnology **32**, 042002 (2020).
[33] R. Jung, M. Metzger, D. Haering, S. Solchenbach, C. Marino, N. Tsiouvaras *et al.*, J. Electrochem. Soc. **163**, A1705–A1716 (2016).
[34] L. Chen, K. Wang, X. Xie, and J. Xie, J. Power Sources **174**, 538–543 (2007).
[35] T. Jaumann, J. Balach, U. Langklotz, V. Sauchuk, M. Fritsch, A. Michaelis *et al.*, Energy Storage Mater. **6**, 26–35 (2017).

[36]M. Ko, S. Chae, and J. Cho, ChemElectroChem **2**, 1645–1651 (2015).
[37]N. Liu, K. Huo, M. T. McDowell, J. Zhao, and Y. Cui, Sci. Rep. **3**, 1919 (2013).
[38]Z. Liu, C. Fang, X. He, Y. Zhao, H. Xu, J. Lei *et al.*, ACS Appl. Mater. Interfaces **13**, 46518–46525 (2021).
[39]Y. Son, J. Sung, Y. Son, and J. Cho, Curr. Opin. Electrochem. **6**, 77–83 (2017).
[40]C. Fang, T.-N. Tran, Y. Zhao, and G. Liu, Electrochim. Acta **399**, 139362 (2021).
[41]J. Wu, F. Ma, X. Liu, X. Fan, L. Shen, Z. Wu *et al.*, Small Methods **3**, 1900158 (2019).
[42]J. D. McBrayer, M.-T. F. Rodrigues, M. C. Schulze, D. P. Abraham, C. A. Apblett, I. Bloom *et al.*, Nat. Energy **6**, 866–872 (2021).
[43]E. J. Hopkins, S. Frisco, R. T. Pekarek, C. Stetson, Z. Huey, S. Harvey *et al.*, J. Electrochem. Soc. **168**, 030534 (2021).
[44]S. Schweidler, L. de Biasi, A. Schiele, P. Hartmann, T. Brezesinski, and J. Janek, J. Phys. Chem. C **122**, 8829–8835 (2018).
[45]Q.-A. Huang, Y. Shen, Y. Huang, L. Zhang, and J. Zhang, Electrochim. Acta **219**, 751–765 (2016).
[46]C. Fang, H. Xiao, T. Zheng, H. Bai, and G. Liu, J. Compos. Sci. **5**, 188 (2021).
[47]H. Xiao, T. Zheng, G. Liu, H. Wang, H. Bai, Y. Fu *et al.*, IOP Conf. Ser.: Earth Environ. Sci. **242**, 042014 (2019).
[48]S. S. Zhang, ChemElectroChem **7**, 3569–3577 (2020).
[49]Y. Yamada, Y. Iriyama, T. Abe, and Z. Ogumi, J. Electrochem. Soc. **157**, A26 (2010).
[50]C. Qian, J. Zhao, Y. Sun, H. R. Lee, L. Luo, M. Makaremi *et al.*, Nano Lett. **20**, 7455–7462 (2020).
[51]M. C. Schulze, G. M. Carroll, T. R. Martin, K. Sanchez-Rivera, F. Urias, and N. R. Neale, ACS Appl. Energy Mater. **4**, 1628–1636 (2021).
[52]Y. Han, P. Qi, X. Feng, S. Li, X. Fu, H. Li *et al.*, ACS Appl. Mater. Interfaces **7**, 2178–2182 (2015).
[53]R. Gao, J. Tang, X. Yu, S. Tang, K. Ozawa, T. Sasaki *et al.*, Nano Energy **70**, 104444 (2020).
[54]Q. Ai, Q. Fang, J. Liang, X. Xu, T. Zhai, G. Gao *et al.*, Nano Energy **72**, 104657 (2020).